JACC: CLINICAL ELECTROPHYSIOLOGY VOL. ■, NO. ■, 2018

Characteristics of Radiofrequency Catheter Ablation Lesion Formation in Real Time In Vivo Using Near Field Ultrasound Imaging

Matthew Wright, MB, BS, PhD,[a] Erik Harks, PhD,[b] Szabolcs Deladi, PhD,[b] Steven Fokkenrood, MSc,[b] Rob Brink, BSc,[b] Harm Belt, PhD,[c] Alexander F. Kolen, PhD,[c] Darrell Rankin, MEng,[d] William Stoffregen, DVM,[d] Debra A. Cockayne, PhD,[d] Joseph Cefalu, BSc,[d] David E. Haines, MD[e]

ABSTRACT

OBJECTIVES Visualizing myocardium with near field ultrasound (NFUS) transducers in the tip of the catheter might provide an image of the evolving pathological lesion during energy delivery.

BACKGROUND Radiofrequency (RF) catheter ablation has been effective in arrhythmia treatment, but no technology has allowed lesion formation to be visualized in real time in vivo.

METHODS RF catheter ablations were performed in vivo with the goal to create transmural atrial lesions and large ventricular lesions. RF lesion formation was imaged in real time using M-mode, tissue Doppler, and strain rate information from the NFUS open irrigated RF ablation catheter incorporating 4 ultrasound transducers (1 axial and 3 radial), and growth kinetics were analyzed. Nineteen dogs underwent ablation in the right and left atria ($n = 185$), right ventricle ($n = 67$), and left ventricle ($n = 66$). Lesions were echolucent with tissue strain rate by NFUS.

RESULTS Lesion growth frequently progressed from epicardium to endocardium in thin-walled tissue. The half time of lesion growth was 5.5 ± 2.8 s in thin-walled and 9.7 ± 4.3 s in thick-walled tissue. Latency of lesion onset was seen in 57% of lesions ranging from 1 to 63.8 s. Tissue edema (median 25% increased wall thickness) formed immediately upon lesion formation in 83%, and intramyocardial steam was seen in 71% of cases.

CONCLUSIONS NFUS was effective in imaging RF catheter ablation lesion formation in real time. It was useful in assessing the dynamics of lesion growth and could visualize impending steam pops. It may be a useful technology to improve both safety and efficacy of RF catheter ablation. (J Am Coll Cardiol EP 2018;■:■–■) © 2018 The Authors. Published by Elsevier on behalf of the American College of Cardiology Foundation. This is an open access article under the CC BY-NC-ND license (http://creativecommons.org/licenses/by-nc-nd/4.0/).

Radiofrequency (RF) catheter ablation has been the mainstay in interventional cardiac electrophysiology. Effective lesion formation has traditionally been assessed with surrogate measures including power, temperature, impedance change, change in electrogram amplitude, contact force, duration of energy delivery, and combinations thereof (1-8). However, direct monitoring of the

From the [a]Division of Imaging Sciences and Biomedical Engineering, King's College London, United Kingdom and Department of Cardiology, St. Thomas' Hospital, London, United Kingdom; [b]Philips Healthcare, Best, the Netherlands; [c]Philips Research, Eindhoven, the Netherlands; [d]Boston Scientific Corporation, San Jose, California; and the [e]Department of Cardiovascular Medicine, Beaumont Health System and Oakland University William Beaumont School of Medicine, Royal Oak, Michigan. Research funding was provided by Philips Healthcare, Best, the Netherlands and Boston Scientific Corporation, Inc., San Jose, California. Dr. Wright and Dr. Haines have received research support from Philips Healthcare and Boston Scientific Corporation. Drs. Harks, Deladi, Betl, and Kolen, Mr. Fokkenrood, and Mr. Brink have been employed by Philips Healthcare. Mr. Rankin, Drs. Stoffregen and Cockayne, and Mr. Cefalu have been employed by Boston Scientific Corporation.

All authors attest they are in compliance with human studies committees and animal welfare regulations of the authors' institutions and Food and Drug Administration guidelines, including patient consent where appropriate. For more information, visit the *JACC: Clinical Electrophysiology* author instructions page.

Manuscript received January 22, 2018; revised manuscript received March 22, 2018, accepted April 12, 2018.

ABBREVIATIONS AND ACRONYMS

RF = radiofrequency

NFUS = near field ultrasound

ICE = intracardiac echocardiography

formation of a pathological lesion has not been possible. Because of the variable efficiency of energy coupling to tissue in the setting of convective cooling by the circulating blood pool and catheter irrigation, it is difficult to know the time course of lesion formation or if a lesion is being created at all. The pattern and kinetics of lesion growth in vivo are unknown because hitherto no methods for direct observation of lesion formation existed during RF catheter ablation.

Ultrasound imaging has shown value in monitoring electrode-tissue contact (9). It has been used to titrate power delivery when excess bubble formation is observed (indicating overheating of the endocardial surface (10). More recently, near-field ultrasound (NFUS) imaging through transducers mounted in the tip of an open-irrigated ablation catheter have been demonstrated to predict steam pops (11) to assess electrode-tissue contact, tissue wall thickness, and RF lesion depth, and transmurality (12,13). It was hypothesized that NFUS imaging of lesion formation in real time would offer insight into the patterns, rates, and magnitude of lesion growth. Thus, monitoring lesion formation with NFUS would be anticipated to facilitate both safety and efficacy of catheter ablation.

METHODS

NEAR FIELD ULTRASOUND ABLATION SYSTEM. The NFUS system has been previously described in detail (13). In brief, the NFUS system is configured with an 8-F catheter using a 5-mm platinum-iridium electrode tip containing 4 single-element piezoelectric ultrasound transducers (c.f. 30 MHz) (1 axial and 3 radial with 120° spacing) and 6 ports for saline irrigation (Boston Scientific Corp., San Jose, California).

RF ablation was performed using a conventional RF ablation generator (Maestro 3000, Boston Scientific Corporation, Marlborough, Massachusetts) and irrigation pump (Cool Flow, Biosense Webster, South Diamond Bar, California). For each individual ultrasound transducer, data were recorded at 100 MHz per line, and lines were sampled at 1 kHz and further processed using custom-built software (Philips Healthcare, Best, the Netherlands). For each transducer, data from M-mode (gray scale), tissue Doppler (red-yellow-cyan-blue color scale), and strain rate (black-orange-blue scale) for each transducer in the catheter tip were displayed with a refreshing fast sweep display (50 mm/s) and an adjacent slow sweep showing a fixed 30- to 150-s time window.

ANIMAL MODEL. The experimental protocol was approved by the Institutional Animal Care and Use Committee of Surpass-Silicon Valley, LLC (Mountain View, California). The facility was in compliance with US Department of Agriculture (USDA) regulations. Canines between 30 and 50 kg in weight were treated with 40-mg sotalol twice daily before the procedure and on the day of the procedure. Anesthesia was induced with ketamine 5 to 10 mg/kg intravenously (IV), diazepam 0.2 to 0.6 mg/kg IV, glycopyrrolate 0.0004 to 0.0008 mg/kg intramuscularly (IM), and buprenorphine 0.01 mg/kg IM and maintained with isoflurane 1% to 2%. Lidocaine, 1 to 2 mg/kg IV and phenylephrine 0 to 5 μg/min IV were used to suppress arrhythmia and maintain blood pressure. Heparin, 50 to 150 mcg/kg IV, was given to maintain an activated clotting time >350 s. Catheter position was monitored with fluoroscopy and electroanatomical mapping (Ensite Velocity, St. Jude Medical). The right femoral, left femoral, and right internal jugular veins and left femoral artery were cannulated for placement of catheters in the coronary sinus, right-sided chambers, and left-sided chambers. Two 8.5-F steerable sheaths (Boston Scientific Corporation) were employed for introduction of a 9-F rotational intracardiac echocardiography (ICE) catheter (Ultra ICE, Boston Scientific Corp.) and the NFUS ablation catheter. ICE imaging was performed with the iLab intracardiac ultrasound imaging console (version 2.5, Boston Scientific Corp.). Transseptal catheterization was guided by ICE and fluoroscopy. The animal was euthanized at termination of the procedure, 30 minutes after the final RF ablation with an overdose of barbiturate.

NEAR FIELD ULTRASOUND CATHETER ABLATION PROTOCOL. The NFUS catheter was manipulated to various sites in all 4 cardiac chambers, and the geometry of each cardiac chamber was recorded by the electro-anatomical mapping system. Catheter location was recorded by 3-dimensional (3D) tagging on the mapping system and by ICE and fluoroscopic imaging. Serial RF ablations were performed at discrete stable catheter positions. The initial power level selected for atrial lesions was 25 to 30 W and for ventricular lesions was 35 to 50 W. Power was titrated up as high as 50 W until lesion formation was observed by NFUS. Irrigation flow rate was 2, 5, or 8 ml/min. Duration of RF energy delivery was 10 to 120 s. The goal was to emulate clinical ablation by attempting to maximize lesion size safely and produce a transmural lesion. RF energy delivery was terminated if transmural lesion formation by NFUS was apparent to the operator, except for cases in which excessive ablation was intentional to produce

FIGURE 1 **RF Lesion Formation in Atrial Tissue**

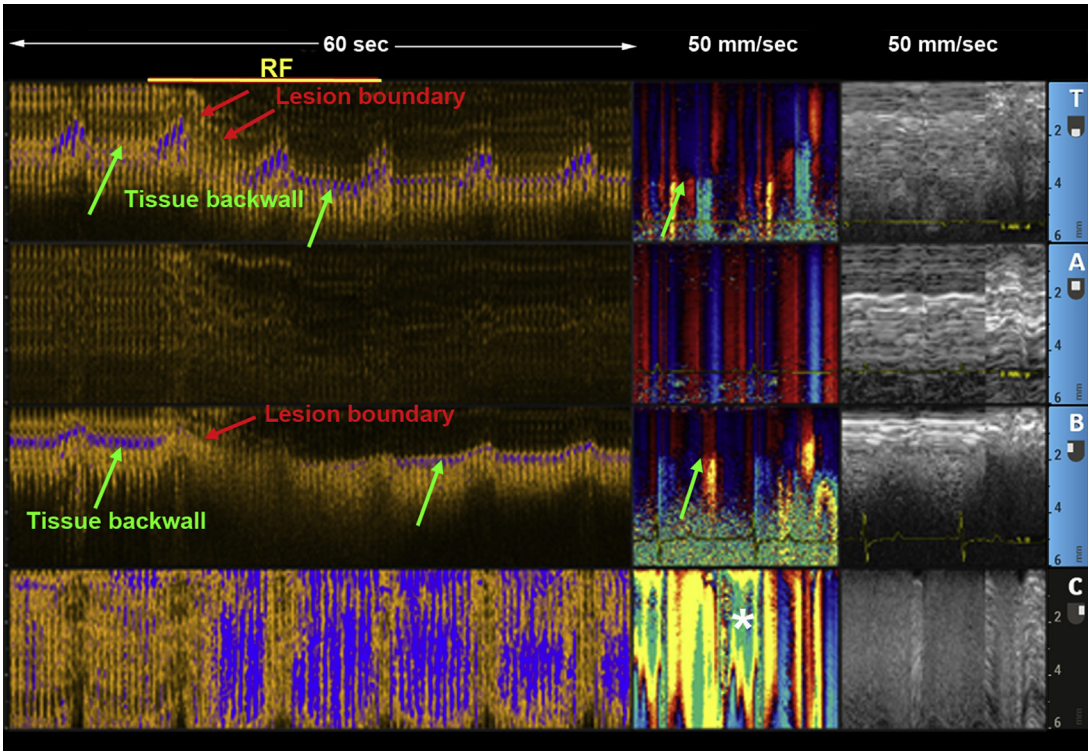

This is an example of RF lesion formation in atrial tissue (right upper pulmonary vein, 35 W. 8 ml/min, 23 s) imaged from the ultrasound transducer at the tip (T), and the 3 circumferential transducers labeled A, B, and C. The **left panels** are the composite trend view over 60 s, and the yellow bar indicates the ablation time. The **middle and right pan**els are real time fast sweep (50 mm/sec) recordings of tissue Doppler and M-mode gray scale, respectively. The imaging transducers at the tip (T) and transducer B show the tissue back wall **(green arrows)** and the progressive change on strain rate that corresponds to the lesion formation **(red arrows)**. The scale bar **(far right)** shows the depth scale measured in millimeters. The **light blue color** of the scale bar indicates good tissue contact on ultrasound transducers T, A, and B. Transducer C **(bottom)** has no contact with the tissue and shows the characteristic disorganized Doppler image of the circulating blood pool **(*)**. Of note, there is significant tissue edema evidenced by a marked increase in wall thickness that occurs over the course of lesion formation.

steam pops. If intramural steam was observed, RF energy delivery was continued without reduction of power to determine if that observation would result in a steam pop. The NFUS images were recorded for post-study analysis off-line.

DATA ANALYSIS. NFUS and ICE images were acquired during the experiments and stored digitally for post-study analysis off-line (Excel, Microsoft Corp, Redmond, Washington). NFUS and ICE images were analyzed by experienced operators blinded to the experimental conditions and the intracardiac catheter locations during image acquisitions. Measurements were made with electronic calipers and stored in an electronic database. The time course and pattern of lesion growth analysis was limited to lesions in which the border of lesion growth over time was clearly apparent on the NFUS image. The lesion edge was traced by a blinded observer then the resulting curve was analyzed for best-fit monoexponential function. Continuous variables are expressed as mean ± SD and were compared among conditions with Student's *t*-tests for normally distributed data and Mann-Whitney U tests for non-normal data. Categorical data were compared with chi-square and Fisher exact tests.

RESULTS

RF lesions monitored with NFUS imaging were created in vivo at varying locations in the right atria (n = 101), left atria (n = 84), right ventricles (n = 67), and left ventricles (n = 66). Examples of NFUS images for typical ablations in atrial (**Figure 1**) and ventricular tissue (**Figure 2**, Online Videos 1 and 2) are shown. The

FIGURE 2 RF Lesion Formation in Ventricular Tissue

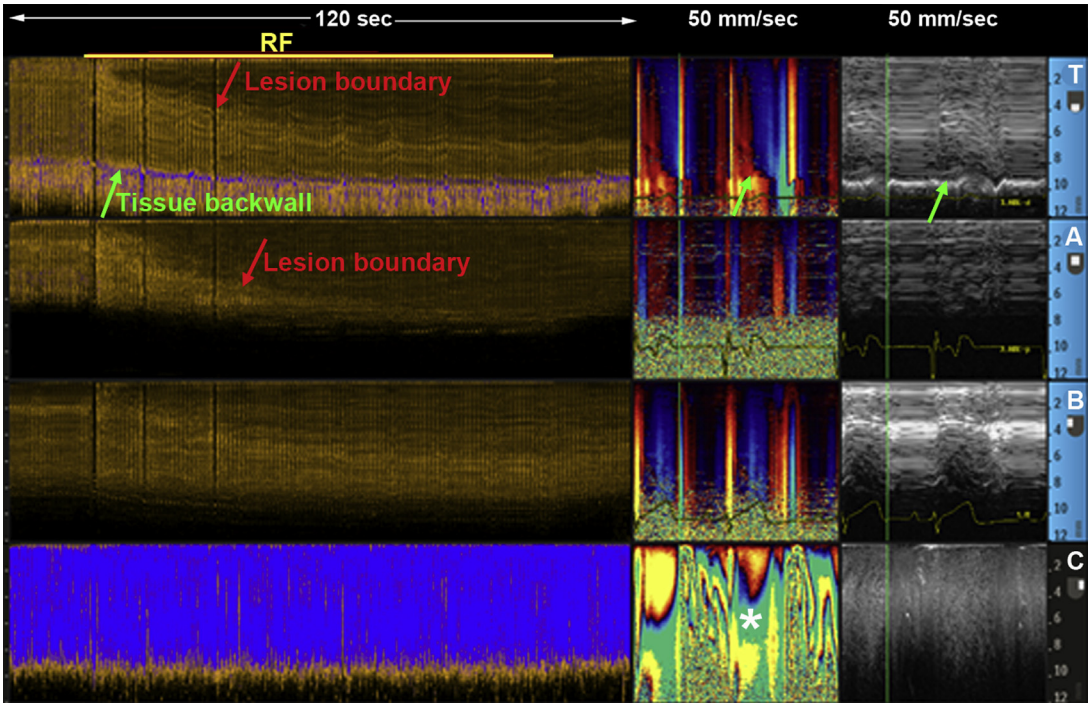

This is an example of RF lesion formation in ventricular tissue (LV lateral wall, 40 W, 8 ml/min, 90 s) presented in the same format as described (see **Figure 1** for details). See Online Videos 1 and 2.

TABLE 1 Biophysical Parameters of Ablation

Location	n	Power (W)	Duration (s)	Impedance Drop (%)	Maximum Temp (°C)	EG Amplitude Drop (%)
RA	101	34 ± 5	44 ± 25	10 ± 4	34 ± 5	47 ± 24
RAA	31	34 ± 5	45 ± 27	11 ± 4	35 ± 6	50 ± 23
Post-wall	46	34 ± 4	45 ± 25	9 ± 4	34 ± 4	44 ± 26
CTI	23	36 ± 5	43 ± 25	12 ± 4	35 ± 5	48 ± 20
LA	84	35 ± 6	43 ± 25	12 ± 5	35 ± 4	40 ± 32
LAA	27	34 ± 5	43 ± 30	11 ± 3	36 ± 6	42 ± 22
MVA	34	36 ± 7	45 ± 25	13 ± 5	34 ± 3	45 ± 29
PV os	23	34 ± 6	38 ± 15	13 ± 5	34 ± 4	29 ± 42
RV	67	45 ± 6	74 ± 30	15 ± 4	34 ± 3	38 ± 39
OT	28	44 ± 7	59 ± 26	14 ± 3	34 ± 3	42 ± 27
FW	22	46 ± 6	81 ± 28	17 ± 4	35 ± 3	23 ± 53
IVS	17	48 ± 4	88 ± 30	16 ± 4	34 ± 3	53 ± 26
LV	66	46 ± 5	81 ± 24	19 ± 4	33 ± 2	21 ± 41
FW	39	47 ± 5	82 ± 27	19 ± 4	33 ± 2	24 ± 37
IVS	27	46 ± 5	80 ± 18	18 ± 4	34 ± 2	18 ± 47

Values are n or mean ± SD.

CTI = cavo-tricuspid isthmus; FW = free wall; IVS = interventricular septum; LA = left atrial; LAA = left atrial appendage; LV = left ventricular; MVA = mitral valve area; OT = outflow tract; PV os = pulmonary vein ostium; RA = right atrial; RAA = right atrial appendage; RV = right ventricular.

measured ablation parameters at each of the ablation sites are detailed in **Table 1**. RF lesions that previously have been demonstrated to correlate with pathological lesions (13) were characterized by a clear demarcation between normal tissue echogenicity in healthy tissue and decreased echogenicity in ablated tissue on gray-scale imaging. The ablated tissue also demonstrated decreased tissue Doppler strain rate compared with normal tissue. For ablations performed at thicker wall ventricular sites, lesion depth determined by NFUS correlated with parameters of lesion formation including power ($p < 0.001$, $r = 0.58$), ablation duration ($p < 0.001$, $r = 0.40$), relative impedance fall during ablation ($p < 0.001$, $r = 0.42$).

DYNAMIC LESION GROWTH. The determination of the time course of lesion growth was limited to a subset of 212 lesions in which the leading edge of lesion formation was clearly discernible upon onset of RF energy delivery. Of these, 93 were from the atria and had wall thicknesses <3 mm (thin wall), 18 were from the atria with wall thicknesses >3 mm, 49 were from the right ventricle, and 52 were from left ventricle. The half-time of lesion growth in the thin

FIGURE 3 **RF Lesion Formation in the Left Atrial Appendage**

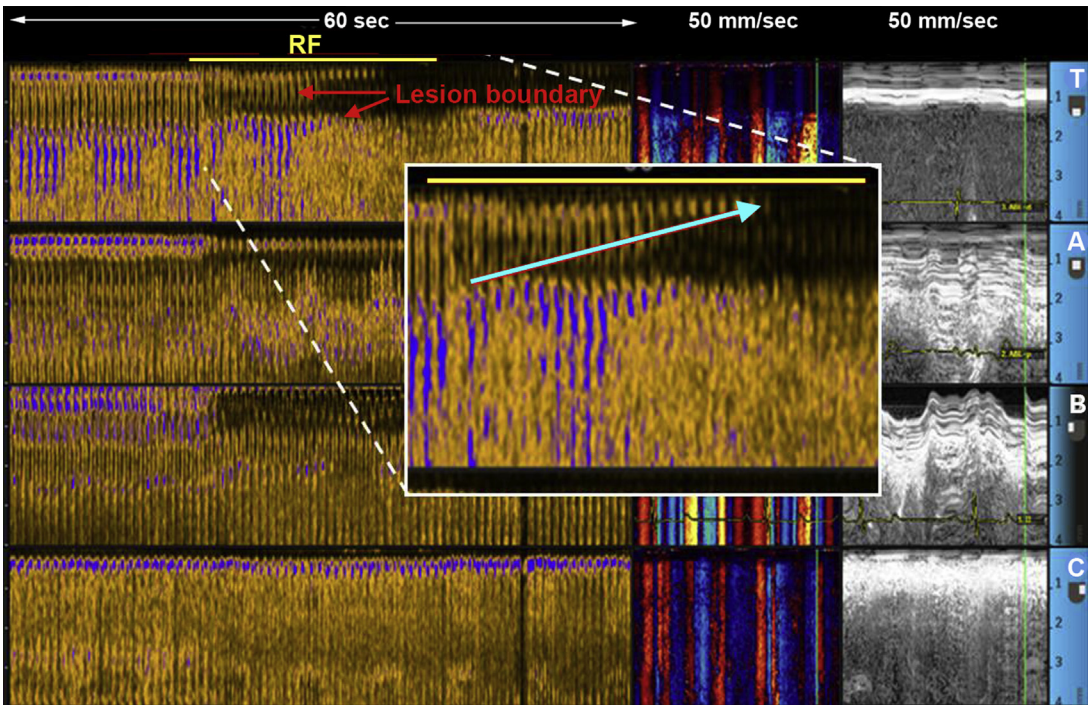

This is an example of ablation in the left atrial appendage (35 W, 5 ml/min, 25 s) presented in the same format previously described (see **Figure 1** for details). There is clear indication of lesion formation recorded by the tip (T) and B transducers, but the tip transducer shows a pattern of lesion growth from the subepicardium back to the endocardial surface **(inset, blue arrow)**. This phenomenon likely occurs because of the endocardial cooling by catheter irrigation and circulating blood pool with subsequent delay in endocardial lesion formation. See Online Videos 3 and 4.

wall atrial samples was 5.5 ± 2.8 seconds, with a wide range from 0.3 to 14.5 s. For the thicker atrial and the ventricular lesions, the half-time of lesion growth was 9.7 ± 4.3 s, with a range of 2.0 to 19.2 s, equating to a mean time to complete lesion formation (5 half-times) of 49 s (range 10 to 96 s). The half-time of lesion growth showed no meaningful correlation with any of the biophysical parameters of ablation (including power, impedance change, and peak temperature) except for a strong correlation with total ablation time ($R = 0.86$). This would be predicted by the experimental design, as RF power delivery was continued until a complete or transmural lesion was observed. Thus, slower-growing lesions, by design, had longer durations of RF power delivery. NFUS imaging suggested that lesions typically formed first in the subendocardium and progressed to deeper tissue planes over time. However, a pattern of lesion growth repeatedly observed, particularly with ablation at thin-wall atrial sites, was midmyocardial or subepicardial initiation with lesion progression to the subendocardial layer (**Figures 3 and 4**, Online Videos 3 and 4). This deep-to-shallow pattern was seen in 61% of ablations in thin-wall atria, 22% in thicker-wall atria, and 17% in left or right ventricles.

ABLATION LATENCY. A delay in the onset of lesion formation as defined by NFUS was frequently observed. Ablation latency ≥1 s was seen in 57% of the ablations, with a median of 2.6 s and a range from 1 to 63.8 s. In addition, a threshold effect was seen during RF ablation where no visualization of lesion formation was observed at lower-power delivery for 30 s or longer; then, with a 5- to 10-W increase in power, lesion formation would begin (**Figure 5**).

TISSUE EDEMA. Lesions created in the atria and right ventricles in the subset of lesions described above were assessed for the appearance of myocardial edema, defined as an increase in myocardial-wall thickness during RF ablation. Ablations in the left ventricle were not analyzed for edema because the limited depth of penetration of NFUS precluded consistent visualization of ventricular-wall thickness. The time course of formation of edema exactly

FIGURE 4 **RF Lesion Formation in the Right Ventricle**

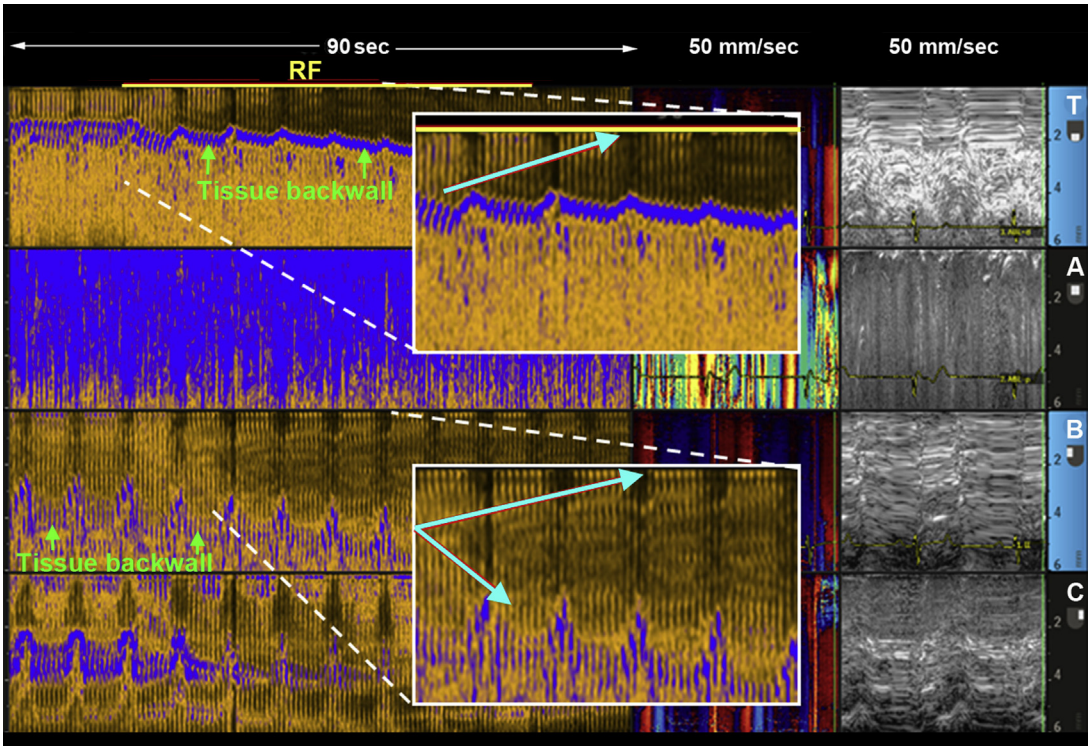

This is an example of ablation of the RV free wall (35 W, 5 ml/min, 60 s) presented in the same format as previously described (see **Figure 1** for details). Lesion formation is apparent on the recordings from transducers T and B and shows a pattern of lesion growth from the subepicardium (T) and midmyocardium (B) back to the endocardial surface **(insets, blue arrows)**. See Online Videos 3 and 4.

mirrored the time course of formation of lesions (see Tip transducer, **Figure 2**). Tissue edema was observed in 83% of lesions, with a 25% median increase of wall thickness in response to ablation (interquartile range: 10% to 48%). Lesions with edema were had a greater impedance drop with energy delivery (13.3%) and a shorter median duration of RF energy delivery (38 s) compared with those without significant edema (11.4%, $p = 0.008$, and 60 s, $p = 0.003$, respectively). However, no differences were observed between groups regarding power, lesion depth, location of lesion, or tissue thickness.

DETECTION OF STEAM POPS WITH NFUS. Steam pops occur during RF catheter ablation when the intramural temperature exceeds 100°C and boiling of tissue water results in formation of steam with sudden venting of the steam bubble through the myocardial surface. This venting may be observed as a sudden burst of intra-atrial bubbles by ICE or as endocardial disruption at pathological examination. Intramural microbubbles are very echogenic and are often visible before the steam pop occurs (**Figure 6**). During 24 ablations, myocardial steam was visualized by NFUS either as premonitory intramyocardial echogenicity at a constant depth appearing 37 ± 19 s prior to steam venting ($n = 18$) or as an abrupt increase immediately before release of steam or termination of delivery of energy ($n = 6$). In 6 additional cases, there was evidence of steam venting but no premonitory myocardial echogenicity (sensitivity for pop or near-pop lesion: 71%). Fifteen cases showed evidence of endocardial disruption by sudden release of steam on gross pathology (**Table 2**). In only 1 instance was the steam pop felt and heard by the operator. Compared with RF lesions with no evidence of steam pops by ICE or pathological examination, RF lesions associated with steam pops were produced with higher power (47 ± 5 W vs. 38 ± 8 W, $p < 0.001$), longer duration of ablation (68 ± 27 s vs. 56 ± 31 s, $p = 0.005$), and were primarily ventricular in location (22 left ventricular, 7 right ventricular, and 1 left atrial). Among lesions with intramyocardial steam visualized

FIGURE 5 **Demonstration of RF Ablation Latency and the Threshold Effect**

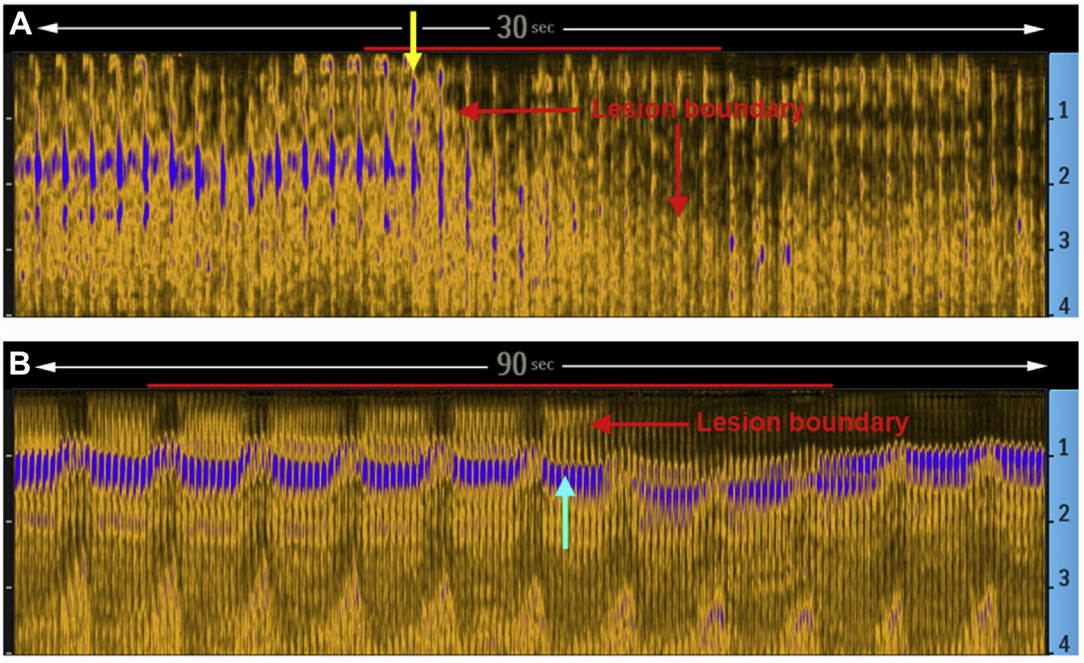

A demonstrates an example of RF ablation latency. The RF energy delivery starts at the onset of the red bar, which indicates the 11-s ablation time (35 W; 8 ml/min), yet the beginning of lesion formation is not observed until 3 s after onset of ablation **(yellow arrow)**. **B** is an example of the threshold effect. During RF ablation at a power of 30 W at 8 ml/min, no lesion formation is observed during the initial 36 s. At 36 s **(blue arrow)**, the power was increased to 35 W, and epicardial-to-endocardial lesion growth begins immediately. Both lesions were created in the right atrium at the SVC-IVC line.

by NFUS, there was no significant difference in power or duration of ablation between lesions with or without steam pops evident on echocardiography or pathological examination. Similarly, no difference between groups was seen regarding the number of transducers in contact with the tissue (a surrogate for catheter compression into tissue).

DISCUSSION

NFUS imaging has been proposed as a technology to monitor real-time lesion formation during RF catheter ablation. Using an array of ultrasound transducers at the catheter tip, growth of the myocardial lesion could be visualized in real time during delivery of RF energy. This was made possible by the difference in properties and motion between healthy and ablated tissue (14). The resultant strain rate image was able to represent the RF lesion formation over time. The lesion depth as observed by NFUS imaging correlated with ablation parameters including power, duration of ablation, and relative fall of impedance during delivery of energy. These correlations were anticipated, as a strong association between NFUS depth of lesion and pathological depth of lesion has been previously reported (13), and the parameters of power, duration, and impedance drop are well established as predictors of size of lesion.

The time course of lesion formation was highly variable. This was hypothesized to be attributable to variations in electrode contact force and sliding catheter contact. The average half-time of lesion growth for thin-walled atrial ablation targets was 5.5 s, suggesting that ablation may be highly effective even with relatively short (<10 s) ablation durations when the target is the posterior left atrium. Shorter RF ablation duration may, in turn, reduce the risk of collateral injury to noncardiac structures. An observation that has never previously been demonstrated in vivo is that in more than one-half of the ablations of thin-walled tissue, lesion growth started in the subepicardium or midmyocardium and progressed to the endocardium over the course of ablation. This could be explained based on the fact that active and

FIGURE 6 **Steam Pop**

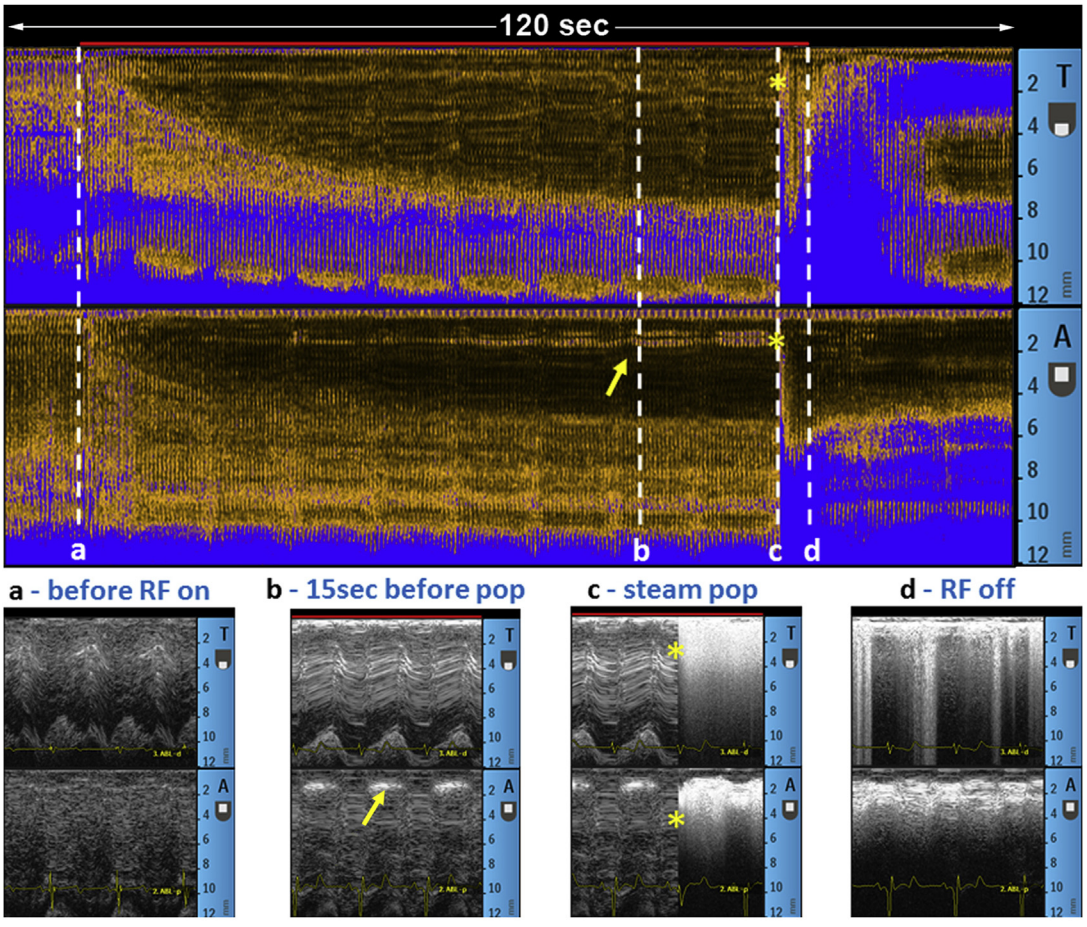

This is an example of an RF ablation on the interventricular septum of the left ventricle, resulting in a steam pop. The NFUS recordings are presented in a similar format as described in Figure 1, except that excerpts of the fast-sweep recordings corresponding to different times on the slow sweep display **(a to d)** are presented separately in the bottom row. The **blue color** of the scale bar **(far right)** indicates good tissue contact on ultrasound transducers T and A. The **red bar** indicates the 84-second ablation time (40 W; 8 ml/min). The sudden increase in echogenicity of the tissue indicates sudden intramyocardial boiling and release of a steam pop **(*)**. Several seconds before this occurrence, intramyocardial echogenicity is apparent **(arrow)**, corresponding to the early formation of steam bubbles.

passive convective cooling spares ablation of the endocardium, whereas RF heating continues in deeper tissue planes. This phenomenon was demonstrated in a model of left atrial ablation in swine. Maximal lesion diameter was observed at the endocardial surface with low irrigation flow rates, but with high irrigation flow rates, the maximal diameter was at the epicardial surface (15). Therefore, surface cooling during ablation could lead to an unintended consequence of heating tissue beyond the epicardium (e.g., the esophagus) and the targeted myocardium.

Latency in onset of lesion formation was frequently observed. The mechanism for this is unknown but may relate to improvement in catheter-tissue contact after onset of ablation due to myocardial stunning and decrease in local tissue motion or improved catheter stability from other mechanisms. It is also possible that the characteristic echocardiographic changes that we correlate with formation of lesions may not represent the full extent of the lesion and that border-zone tissue starts to become ablated before actual visualization by NFUS, resulting in latency of the appearance of the lesion by NFUS. A threshold effect for power titration and lesion formation was also observed. A modest increase in power during RF ablation could cause a sudden

transition from no visible lesion to active lesion formation. This indicates that the power and lesion size relationship is not proportional for individual lesions. The mechanism behind this observation is unknown but, again, may be the result of myocardial stunning, leading to improved energy coupling between the electrode and tissue and more effective RF ablation.

The importance of achieving an effective ablation on the first attempt has long been recognized, and performing sequential contiguous lesions has been identified as a predictor for successful pulmonary vein isolation (7). The difficulty in successfully reablating at sites of ablation performed earlier in procedures has been attributed to tissue edema that leads to swelling and thickening of the target tissue, making transmural ablation more difficult. Although the presence of myocardial edema has been well characterized (16), the time course of its formation has previously been unknown. In the current study, edema was observed to accumulate immediately and, coincident with lesion formation, resulting in a median 25% increase in tissue thickness. Predictors of formation of edema were a greater impedance drop, suggesting faster/more heating. By protocol design, ablation was terminated when transmurality or steady-state lesion size was achieved; therefore, it was anticipated that shorter lesion durations were seen in lesions with significant edema formation, as these probably represented ablations with more efficient energy coupling between the catheter and the tissue.

Sudden rises in electrical impedance have been attributed to the temperature exceeding 100°C at the electrode-tissue interface with boiling of plasma and denaturation of blood proteins (17). With active irrigation, the highest temperature is achieved 3 to 4 mm below the endocardial surface, and in cases of excess RF energy delivery, the tissue water will boil. This can lead to sudden steam expansion and so-called pop lesions as the steam is suddenly vented to the tissue surface. In the worst case, this can cause perforation and pericardial tamponade. NFUS was able to image impending steam pops in 71% of cases. If the study had been designed to allow immediate termination of RF energy delivery upon intramural microbubble formation, it is likely that the majority of steam pops could have been avoided, thus enhancing the safety of this procedure.

TABLE 2 Correlation of Intramyocardial Steam Formation to Evidence of Steam Pop

NFUS and echocardiographic observations	Pathological Evidence of Endocardial Disruption by Steam Pop: Present	Absent	Total
Intramural echogenicity, abrupt increase in echo contrast, sudden venting	12	5	17
Intramural echogenicity, abrupt increase in echo contrast, no venting	1	0	1
No intramural echogenicity, abrupt increase in echo contrast, sudden venting	2	1	3
No intramural echogenicity, abrupt increase in echo contrast, no sudden venting	0	3	3
No intramural echogenicity, no abrupt increase in echo contrast, no sudden venting	0	288	288

NFUS = near field ultrasound.

DYNAMICS OF RF LESION FORMATION. Successful catheter ablation depends on a critical balance between efficacy and safety. A successful RF lesion needs to incorporate the targeted tissue completely and result in irreversible cellular injury and death of that tissue. Therefore, ablation efficacy favors large and deep lesion formation. Unfortunately, critical structures often lie just beyond the target tissue. For example, posterior left atrial wall thickness can be less than 2 mm, and the esophagus is frequently immediately contiguous to the left atrial ablation site. As a result, atrial esophageal fistula has proved to be a vexing complication of atrial fibrillation ablation procedures (18,19). To maximize efficacy and safety, a variety of surrogate measures for lesion formation have been employed, including surface temperature sensing (20), electrical impedance (6), and electrogram amplitude (21). Although very useful, these parameters are imprecise and do not inform on ultimate lesion completion. The wide adoption of force-sensing technology may have improved the efficacy of lesion formation because good coupling of energy delivery to the tissue can be assured, but control and monitoring of the evolving lesion is not possible. NFUS has the distinct advantage over these approaches in that actual lesion formation can be observed directly. If no lesion is visible by NFUS, one may reasonably conclude that no lesion is being produced, probably because of poor contact, inadequate power, excess convective cooling, or combinations thereof. It might be possible to ablate deeper extracardiac structures with complete sparing of the thin myocardial wall in contact with the irrigated catheter. Ablation safety can be enhanced with NFUS by terminating ablation when transmurality has been achieved. Also, as increased echogenicity typically precedes rapid steam expansion (pop) by at least 5 s (11), it is anticipated that steam pops could be substantially

mitigated by termination of power immediately when increasing contrast is observed.

STUDY LIMITATIONS. Catheter ablation in the animal model may not accurately represent human catheter ablation, so the data derived from NFUS imaging may not be exactly representative of what would be observed in patients. Because systematic dose ranging of ablation power was not performed, there were relatively few unsuccessful or incomplete lesions produced. Therefore, determination of the specificity of NFUS for the prediction of pathological lesion formation is not possible from the current data set. It is likely that variability in catheter contact force between and during ablations accounted for substantial variability in the efficiency of lesion production, but this could not be measured with the current ablation system (nor can sliding contact be assessed by contact force measurement). The data set used to determine the time course of lesion formation was limited to ablation where the expanding lesion border was clearly discernible in the initial 10 seconds of ablation (64%). The reason for increased acoustical noise and decreased image resolution at the onset of energy delivery in some cases was radiofrequency electrical interference. This was corrected in later versions of the system. The patterns of lesion growth that are hypothesized in this study may be specific to this model, to the healthy cardiac tissue inherent in the healthy canine model, or to the ablation parameters selected for this study and may not represent what occurs during clinical ablation. Additional complexities contributing to 3D lesion development cannot be excluded. The study was designed to determine the sensitivity of NFUS for pop lesions, and therefore power delivery was continued despite the observation of intramyocardial steam formation. Although it is hypothesized that early cessation of power delivery upon observation of intramyocardial echo contrast will reduce the risk of steam pops, this was not tested in the current protocol.

CONCLUSIONS

Maximizing efficacy and safety during RF catheter ablation remains an overarching goal. Surrogate markers of lesion formation have lacked both sensitivity and specificity in achieving this goal. NFUS is the first technology that allows the operator to observe the formation of the RF lesion in real time and to adjust ablation parameters to optimize lesion formation. It is able to successfully predict lesion transmurality and guide the operator's adjustment of ablation parameters in real time during ongoing ablation. Use of NFUS to guide clinical catheter ablation is anticipated to improve both procedural success and procedural safety.

ADDRESS FOR CORRESPONDENCE: Dr. David E. Haines, Oakland University William Beaumont School of Medicine, Heart Rhythm Center, Beaumont Health System, 3601 West 13 Mile Road, Royal Oak, Michigan 48073. E-mail: dhaines@beaumont.edu.

PERSPECTIVES

COMPETENCY IN MEDICAL KNOWLEDGE: Know the pathophysiology of RF lesion formation during catheter ablation of ventricular myocardium.

TRANSLATIONAL OUTLOOK: The current study offers a unique insight into actual real-time radiofrequency catheter ablation lesion formation in vivo. These observations will help operators optimize ablation methods and technologies. To be used in the clinical setting, an approved commercial product must be developed. For this to be a useful clinical tool, much of the system and image analysis will need to be simplified. The time, effort, and money required to achieve this goal may preclude its introduction into clinical investigation. Nonetheless, it is hoped that lessons learned in preclinical studies will be directly applicable to activities in the clinical laboratory.

REFERENCES

1. Wittkampf FH, Hauer RN, Robles de Medina EO. Control of radiofrequency lesion size by power regulation. Circulation 1989;80:962–8.

2. Yuyun MF, Stafford PJ, Sandilands AJ, et al. The impact of power output during percutaneous catheter radiofrequency ablation for atrial fibrillation on efficacy and safety outcomes: A systematic review. J Cardiovasc Electrophysiol 2013;24:1216–23.

3. Nath S, DiMarco JP, Haines DE. Basic aspects of radiofrequency catheter ablation. J Cardiovasc Electrophysiol 1994;5:863–76.

4. Petersen HH, Chen X, Pietersen A, et al. Temperature-controlled radiofrequency ablation of cardiac tissue: An in vitro study of the impact of electrode orientation, electrode tissue contact pressure and external convective cooling. J Interv Card Electrophysiol 1999;3:257–62.

5. Holmes D, Fish JM, Byrd IA, et al. Contact sensing provides a highly accurate means to titrate radiofrequency ablation lesion depth. J Cardiovasc Electrophysiol 2011;22:684–90.

6. Reichlin T, Lane C, Nagashima K, et al. Feasibility, efficacy, and safety of radiofrequency ablation of atrial fibrillation guided by monitoring of the initial impedance decrease as a surrogate of catheter contact. J Cardiovasc Electrophysiol 2015;26:390–6.

7. Kuck KH, Reddy VY, Schmidt B, et al. A novel radiofrequency ablation catheter using contact force sensing: Toccata study. Heart Rhythm 2012;9:18–23.

8. Ikeda A, Nakagawa H, Lambert H, et al. Relationship between catheter contact force and

radiofrequency lesion size and incidence of steam pop in the beating canine heart: electrogram amplitude, impedance, and electrode temperature are poor predictors of electrode-tissue contact force and lesion size. Circ Arrhythm Electrophysiol 2014;7:1174–80.

9. Okumura Y, Johnson SB, Bunch TJ, et al. A systematical analysis of in vivo contact forces on virtual catheter tip/tissue surface contact during cardiac mapping and intervention. J Cardiovasc Electrophysiol 2008;19:632–40.

10. Kilicaslan F, Verma A, Saad E, et al. Transcranial Doppler detection of microembolic signals during pulmonary vein antrum isolation: implications for titration of radiofrequency energy. J Cardiovasc Electrophysiol 2006;17:495–501.

11. Wright M, Harks E, Deladi S, et al. Visualizing intramyocardial steam formation with a radiofrequency ablation catheter incorporating near-field ultrasound. J Cardiovasc Electrophysiol 2013;24:1403–9.

12. Wright M, Harks E, Deladi S, et al. Real-time lesion assessment using a novel combined ultrasound and radiofrequency ablation catheter. Heart Rhythm 2011;8:304–12.

13. Haines DE, Wright M, Harks E, et al. Near field ultrasound imaging during radiofrequency catheter ablation I: assessment of lesion depth, tissue thickness and epicardial wall visualization. Circ Arrhythm Electrophysiol 2017;10:e005295. https://doi.org/10.1161/CIRCEP.117.005295.

14. Kwiecinski W, Provost J, Dubois R, et al. Quantitative evaluation of atrial radio frequency ablation using intracardiac shear-wave elastography. Med Phys 2014;41:112901. https://doi.org/10.1118/1.4896820.

15. Kumar S, Romero J, Stevenson WG, et al. Impact of lowering irrigation flow rate on atrial lesion formation in thin atrial tissue. Preliminary observations from experimental and clinical studies. J Am Coll Cardiol EP 2017;3:1114–25.

16. Arujuna A, Karim R, Caulfield D, et al. Acute pulmonary vein isolation is achieved by a combination of reversible and irreversible atrial injury after catheter ablation: evidence from magnetic resonance imaging. Circ Arrhythm Electrophysiol 2012;5:691–700. https://doi.org/10.1161/CIRCEP.111.966523.

17. Haines DE, Verow AF. Observations on electrode-tissue interface temperature and effect on electrical impedance during radiofrequency ablation of ventricular myocardium. Circulation 1990;82:1034–8.

18. Knopp H, Halm U, Lamberts R, et al. Incidental and ablation-induced findings during upper gastrointestinal endoscopy in patients after ablation of atrial fibrillation: a retrospective study of 425 patients. Heart Rhythm 2014;11:574–8.

19. Zellerhoff S, Ullerich H, Lenze F, et al. Damage to the esophagus after atrial fibrillation ablation: just the tip of the iceberg? High prevalence of mediastinal changes diagnosed by endosonography. Circ Arrhythm Electrophysiol 2010;3:155–9.

20. Bruce GK, Bunch TJ, Milton MA, et al. Discrepancies between catheter tip and tissue temperature in cooled-tip ablation: relevance to guiding left atrial ablation. Circulation 2005;112:954–60.

21. Otomo K, Uno K, Fujiwara H, et al. Local unipolar and bipolar electrogram criteria for evaluating the transmurality of atrial ablation lesions at different catheter orientations relative to the endocardial surface. Heart Rhythm 2010;7:1291–300.

KEY WORDS catheter ablation, lesion formation, ultrasound, atrial fibrillation

APPENDIX For supplemental videos, please see the online version of this paper.